



HAL
open science

Impacts of the hydroxyls crosslinking on lignin softening and pyrolysis via in situ ^1H NMR, rheology, DRIFT and SPI-MS

Zhiguo Dong, Anthony Dufour, Richard Laine, Sebastien Leclerc, Liangyuan Jia, Yingquan Chen, Xianhua Wang, Hanping Chen, Haiping Yang

► To cite this version:

Zhiguo Dong, Anthony Dufour, Richard Laine, Sebastien Leclerc, Liangyuan Jia, et al.. Impacts of the hydroxyls crosslinking on lignin softening and pyrolysis via in situ ^1H NMR, rheology, DRIFT and SPI-MS. *Fuel Processing Technology*, 2022, 236, pp.107390. 10.1016/j.fuproc.2022.107390 . hal-03736217

HAL Id: hal-03736217

<https://hal.univ-lorraine.fr/hal-03736217v1>

Submitted on 22 Jul 2022

HAL is a multi-disciplinary open access archive for the deposit and dissemination of scientific research documents, whether they are published or not. The documents may come from teaching and research institutions in France or abroad, or from public or private research centers.

L'archive ouverte pluridisciplinaire **HAL**, est destinée au dépôt et à la diffusion de documents scientifiques de niveau recherche, publiés ou non, émanant des établissements d'enseignement et de recherche français ou étrangers, des laboratoires publics ou privés.

1 **Impacts of the hydroxyls crosslinking on lignin softening and pyrolysis via *in situ***

2 **¹H NMR, rheology, DRIFT and SPI-MS**

3 *Zhiguo Dong^{a,b}, Anthony Dufour^{b*}, Richard Laine^b, Sebastien Leclerc^c, Liangyuan Jia^d,*

4 *Yingquan Chen^a, Xianhua Wang^a, Hanping Chen^a, Haiping Yang^{a*}*

5 ^a State Key Laboratory of Coal Combustion, School of Energy and Power Engineering,

6 Huazhong University of Science and Technology, Wuhan, 430074, China

7 ^b LRGP, CNRS, Université de Lorraine, ENSIC, 1 rue Grandville 54000 Nancy, France

8 ^c LEMTA (UMR 7563)–CNRS–Université de Lorraine, Vandoeuvre-lès-Nancy,

9 France

10 ^d School of Chemistry and Chemical Engineering, Hefei University of Technology,

11 Hefei, Anhui 230009, China

12 **Abstracts:**

13 The softening and foaming of lignin during pyrolysis are the main obstacles to the
14 scale-up of lignin pyrolysis systems. In this study, the mechanism of borate
15 crosslinking on lignin softening and pyrolysis process was investigated by combining
16 *in-situ* physical and chemical techniques. First, the mobile protons and visco-elastic
17 modulus during lignin pyrolysis were quantitatively analyzed by *in-situ* high
18 temperature ¹H NMR and rheology. It was found that the maximum content of mobile
19 protons during the pyrolysis of raw lignin is around 90%. Hydroxyl crosslinking greatly
20 inhibits the formation of mobile protons. The raw lignin produces a soft material from
21 about 150 °C and starts to form a more rigid material from 200 °C. At 210 °C ~ 330 °C,
22 mobile liquid-like intermediates are entrapped in the rigid char, forming “cavities”.
23 With the addition of boron, the viscoelasticity tends to be stable and mainly elastic.
24 Then, *in-situ* diffuse reflectance infrared Fourier transform spectroscopy and single
25 photoionization time-of-flight mass spectrometry were used to characterize the

26 evolution of functional groups and volatiles. It was found that the shielding of hydroxyl
27 groups by borate inhibits the decomposition of lignin but improves the selectivity to
28 phenols, and more oxygenated groups remain in the char.

29

30 **Keywords:** Lignin; Softening; Pyrolysis; Borate; Char

31 **1. Introduction**

32 Lignin resource utilization is of great significance to the construction of green and
33 low-carbon energy structures. Pyrolysis is an attractive technology to convert lignin
34 into high-value chemicals and fuels[1]. However, the adverse effects of lignin
35 softening and foaming on the system mass transfer and product properties are an
36 important issue[2].

37 Several studies have attempted to reveal the origin of lignin softening and its
38 influence on pyrolysis. Shrestha et al.[3] found that the softening of lignin is due to
39 glass phase transition overlapped with the scission of covalent bonds, giving more
40 low molecular weight mobile species. Tiarks et al.[4] observed that lignin underwent
41 the whole process of melting, agglomeration, ejection, and volatilization using
42 imaging, and pointed out that liquid coalescence was the main reason for the droplet
43 thermal ejection. Zhou et al.[5] has even found that thermal ejection of liquid
44 intermediates was the main way to form pyrolytic lignin. Dufour et al.[6] pointed out
45 that isolated lignin was more mobile than in native lignocellulosic biomass because
46 more interactions between polymers occur in the natural biomass network. Kubo et
47 al.[7] studied the non-covalent hydrogen bonding in lignin and found that
48 intermolecular hydrogen bonds formed between bisphenol and phenol moieties could
49 reduce the thermal mobility of lignin, but they also found that phenolic hydroxyl
50 groups are more difficult to form hydrogen bonds than aliphatic hydroxyl groups.

51 Therefore, properly strengthening molecular interactions, such as cross-linking, would
52 likely improve lignin pyrolysis.

53 Xin et al.[8] reported that torrefaction pretreatment of lignin could promote the
54 crosslinking and condensation of lignin and then prevent the bed agglomeration
55 during pyrolysis. Ghysels et al.[9] mixed 20% calcium hydroxide with lignin, and
56 found that calcium hydroxide could form bridging bonds between the two hydroxyl
57 groups of lignin, which inhibited the agglomeration of char with more monomers
58 produced. Magnesium hydroxide and calcium carbonate have also been found to have
59 a similar action mechanism on lignin[10, 11]. However, the crosslinking efficiency of
60 these modification methods is lower. Boron compounds (boric acid or borates), as a
61 kind of highly efficient hydroxyl crosslinking agents, have been used to speed up the
62 stabilization of lignin-based carbon fibers[12]. Our previous study also found that
63 boron compounds could inhibit the char agglomeration during the pyrolysis of lignin,
64 and boron-doped carbon nanospheres were obtained[13]. However, how the
65 interactions between borate and lignin may improve the softening and pyrolysis of
66 lignin is poorly understood.

67 *In situ* non-invasive analysis is very important to reveal the pyrolysis mechanism of
68 biomass. For example, Dai et al.[14] studied the pyrolysis mechanism of
69 hemicellulose by *in situ* diffuse reflectance infrared Fourier transform spectroscopy
70 (DRIFT) and TG-PIMS. However, these methods are not tailored to analyze the
71 physical properties of biomass during pyrolysis. In recent years, in-situ high
72 temperature ¹H NMR and rheology have been used to analyze the matrix mobility and
73 rheological properties during biomass pyrolysis[15]. Therefore, it is necessary to
74 combine these methods to reveal the physical-chemical mechanism of lignin
75 pyrolysis.

76 Hence, in this study, the mechanism of borate crosslinking on lignin softening and
77 pyrolysis was explored. *In situ* ^1H NMR was used for the quantitative analysis of
78 mobile protons during lignin pyrolysis, while rheology was used to study the
79 viscoelastic properties of lignin undergoing thermal conversion. In addition, DRIFT
80 spectroscopy was used to investigate the changes in functional groups during lignin
81 pyrolysis, and a micro-fixed bed reactor combined with single photoionization
82 time-of-flight mass spectrometry (SPI-TOFMS) was used to monitor the release
83 properties of volatiles.

84 **2. Materials and methods**

85 **2.1. Materials**

86 The lignin was alkali lignin extracted from black liquor of papermaking (Shanhu
87 Chemical, Nanjing, China), and its composition and structure are shown in Table S1
88 and S2, respectively. Ammonium borate (>98.9%, $(\text{NH}_4)_2\text{B}_4\text{O}_7 \cdot 4\text{H}_2\text{O}$) was purchased
89 from Sigma-Aldrich.

90 The pretreatment method of lignin was as follows: 1g lignin and different amounts
91 (0, 1%, 3% and 5%) of ammonium borate (BN) were added to 100 mL deionized
92 water, and ultrasonic dispersion (40 kHz, 300 W) was performed at room temperature
93 for 1 h. The mixed solution was then quickly dropped into liquid nitrogen for freezing.
94 Finally, the frozen lignin particles were put into a vacuum freezing dryer and dried for
95 48h.

96 **2.2. In situ analysis of lignin pyrolysis behavior**

97 *In situ* ^1H NMR analysis was performed on a Bruker Avance III HD 300 MHz
98 NMR instrument equipped with a Bruker SEI-HT high-temperature probe (Fig. S1).
99 About 40 mg of lignin was put into an NMR quartz tube (5mm diameter), and then a
100 glass capillary connected to high purity argon gas (10 ml/min) was inserted into the

101 tube to flush out the air. Then the quartz tube was put into the probe. The heating rate
102 of the quartz tube was controlled at 5 °C/min within the temperature range of
103 120~450 °C. Solid echo experiments were recorded at intervals of 10 °C with a 128
104 scan accumulation and a recycle delay of 0.4 s. At each recording point, the probe was
105 manually tuned to counteract temperature changes. MATLAB software was used to
106 deconvolute the spectrum into a Gaussian peak (solid-like) and a Lorentzian peak
107 (liquid-like), and the fitting regression coefficient (R^2) was always higher than 99%
108 (examples are shown in Fig. S2) [6]. The fraction of mobile H protons in the fluid
109 phase can be expressed by using Equation (1):

$$110 \quad \%H_L = A_L / (A_L + A_G) \times 100\% \quad (1)$$

111 where A_L and A_G are the areas of Lorentzian and Gaussian peaks, respectively.

112 *In situ* rheological analysis of lignin was carried out in an ARES G2 high-torque
113 controlled strain rheometer (Fig. S3). About 500 mg of lignin was pressed into pellets
114 with a diameter of 10 mm and a height of about 4 mm. The sample was fixed between
115 two parallel serrated plates, and a vertical static force of 200 g was applied. High
116 purity N_2 was introduced into the furnace to provide an inert atmosphere, and the
117 temperature increased from 90 °C to 450 °C at the heating rate of 5°C/min. Small
118 amplitude of rotational oscillation was applied to the bottom plate with a strain
119 amplitude of 1% and a frequency (ω) of 1 Hz (6.28 rad·s⁻¹). The oscillation of the
120 bottom plate is transmitted through the sample to the upper plate, and its response is
121 calculated to obtain the elastic modulus (G') and viscous modulus (G''). The complex
122 viscosity (η^*) can be calculated from the Equation (2), and $\tan(\delta)$ is given from the
123 Equation (3):

$$124 \quad |\eta^*| = \sqrt{(G'^2 + G''^2)} / \omega \quad (2)$$

$$125 \quad \tan(\delta) = G'' / G' \quad (3)$$

126 where δ ($0 < \delta < \pi/2$) is the phase angle between stress and strain. Where $\tan(\delta) > 1$,
127 the material is mainly viscous, while $\tan(\delta) < 1$ depicts a mainly elastic material.

128 *In situ* DRIFT spectra of lignin pyrolysis were performed on a Bruker Vertex-70
129 FTIR spectrometer equipped with a diffuse reflectance accessory. Lignin was heated
130 from 30 °C to 500 °C at a heating rate of 5 °C/min. The spectra were recorded at 5 °C
131 intervals with a resolution of 8 cm⁻¹ and scanned 64 times per minute. Corresponding
132 scans of pure KBr particles were taken as the background at each recording point. The
133 relative intensity (I_v/I_m) of the functional group given is the ratio of the variable
134 intensity (I_v) to the maximum intensity (I_m).

135 The slow pyrolysis experiment was carried out in a quartz U-shaped micro fixed
136 bed reactor (length 25 mm, i.d. 10 mm) (**Fig. S4**). 200 mg lignin particles were
137 pre-placed on the quartz sieve plate at the bottom of the reactor. N₂ was used as
138 carrier gas with a flow rate of 200 mL /min. The furnace temperature was controlled
139 by electric heating program, rising from 30 °C to 700 °C at a heating rate of 5 °C/min.
140 Thermocouples were inserted into the reactor to monitor the sample temperature. The
141 volatiles were sampled through a quartz capillary transfer line (280 °C) into
142 SPI-TOFMS (Hefei University of Technology, China) for online analysis. The system
143 is equipped with a VUV photoionization lamp module (PKS106, Heraeus, England)
144 with a photon energy of 10.6 eV and a reflection TOF-MS with a mass resolution of
145 4000 [16].

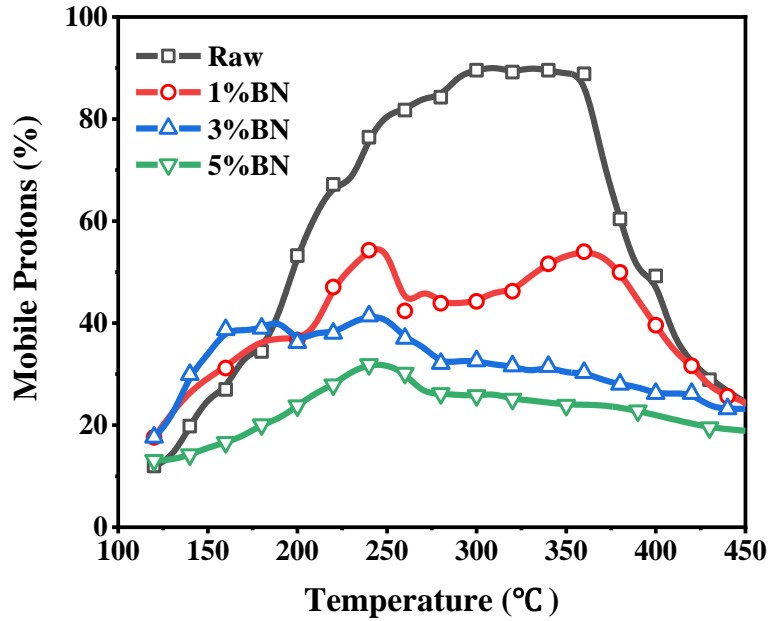
146 **3. Results and discussions**

147 **3.1. Evolution of mobile protons during lignin pyrolysis via in-situ ¹H NMR**

148 The evolution of mobile protons during lignin pyrolysis is shown in **Fig. 1**. For raw
149 lignin, the mobile H content increases gradually from 12% at 120 °C to 90% at 300 °C,
150 remains until 350 °C, then rapidly decreases to 25% at 450 °C. Specifically, at

151 120~300 °C, the mobility of chain segments in lignin increases, and subsequent
152 cleavage of bonds produces more fragments with higher fluidity[6]. The high fluidity
153 at 300~350 °C might be related to the conversion of these fragments. While the rapid
154 decay of mobile H after 350 °C might be due to the devolatilization (loss in H) and to
155 crosslinking reactions [17].

156 With boron addition, the fraction of the fluid phase is reduced substantially. This
157 demonstrates that the cross-linking between borates and lignin chains inhibits the
158 formation of mobile H protons. With the increase of boron content, the maximum
159 mobile proton content decreases. For 1%BN, two peaks (around 54%) of mobile
160 protons appear at 250°C and 350°C, respectively. The former might be related to the
161 motion of chain segments or molecules inside the partly crosslinked structures, while
162 the latter might be due to the depolymerization of chain segments to form a small
163 number of mobile fragments. 3%BN and 5%BN also showed mobile protons peak
164 with decreasing intensity to 41% and 32% around 250 °C respectively, which indicates
165 that the mobility of chain segments becomes more difficult with the increase of
166 crosslinking density. However, there is no peak that occurs around 350 °C for 3%BN
167 and 5%BN, suggesting that the formation of mobile intermediates is considerably
168 inhibited. It is worth noting that the fluidity of 5%BN lignin is lower than the reported
169 fluidity of cellulose (35%) [6].



170

171

Fig.1. Evolution of mobile protons as a function of temperature

172

3.2. Evolution of viscoelastic properties during lignin pyrolysis via in-situ

173

rheology analysis

174

Elastic (G') and viscous (G'') moduli and deformation (displayed between 90 °C and

175

450 °C) of lignin with boron addition are shown in **Fig. 2**. For raw lignin (**Fig. 2a**), the

176

value of G' is higher than G'' between 90 and 130 °C, and there is no obvious

177

deformation of lignin, indicating that lignin is mainly rigid at this temperature range.

178

Then G' is equal to G'' at 150 °C as a mark of the glass phase transition of lignin.

179

Subsequently, lignin swells and then shrinks dramatically. The G' and G'' values

180

decrease, but the higher G'' indicates that lignin has become mainly viscous. It is

181

worth noting that with an increase of 30 °C (from 170 °C to 200 °C), the deformation is

182

as high as 60% (from +30% to -30%). From 200 °C, the G' value increases and is

183

again above G'' , the matrix becomes mainly elastic and the deformation becomes

184

stable. After 300 °C, the G'' value increases, indicating that the important crosslinking

185

reactions happened leading to the resolidification of the matrix. As the temperature is

186

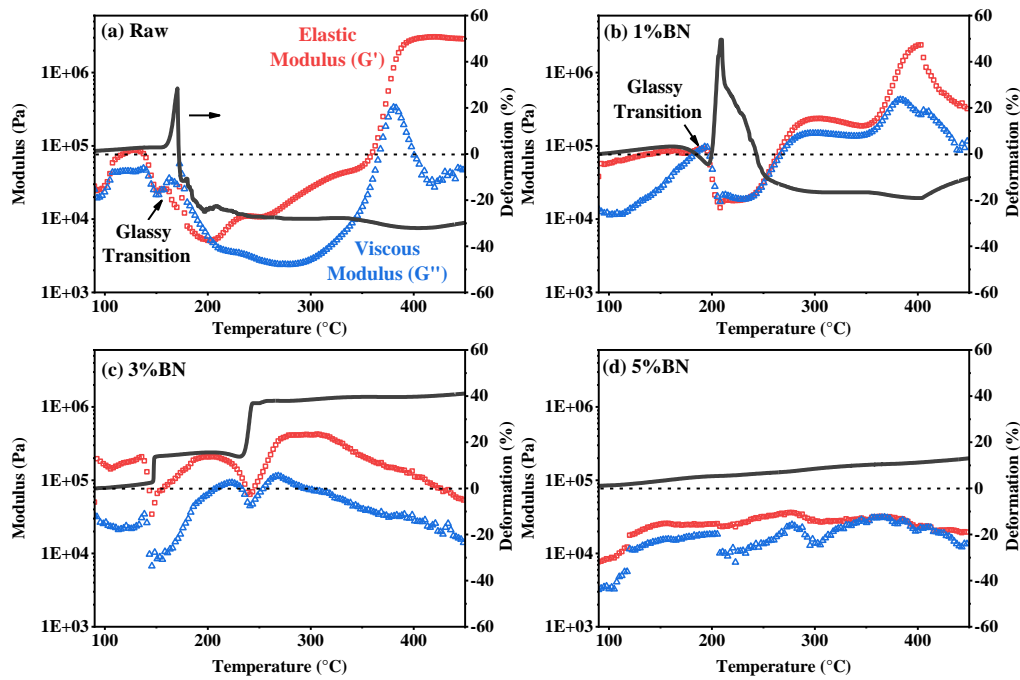
higher than 380 °C, the value of G' (3 MPa) is much greater than that of G'' (0.04

187 MPa). This highlights that the matrix becomes highly rigid, forming a brittle char. All
188 these observations are consistent with our previous work on other lignins [3, 15].

189 With a low boron addition (1%BN), as shown in **Fig. 2b**, the glassy transition of
190 lignin is delayed, and the swelling happens after 200 °C. However, a deformation of 50%
191 is reached, which is higher than that of the raw lignin (30%). At this point, both G'
192 and G'' decrease rapidly, confirming the breaking of interactions within the lignin
193 matrix. Afterward, softening of the matrix occurs in a temperature range of
194 210~250 °C. Both G' and G'' remains stable and then increase, indicating that the
195 interactions within the matrix are strengthened by crosslinking reactions.

196 With boron content increase (3%BN, **Fig. 2c**), the maximum deformation is around
197 40%, while the softening of lignin does not occur. Overall, the value of G' stays
198 higher than G'' and their difference remained constant, indicating that the matrix
199 exhibits mainly elastic properties. It is interesting to note that the lignin exhibits
200 two-step swelling at 150 °C and 230 °C, respectively. Correspondingly, there are two
201 “valleys” on the G' and G'' curves. This implies that there might be two different
202 interactions between borate and lignin, and the proposed interaction mechanism is
203 shown in **Scheme 1**. The tetrahydroxy borate (B(OH)₄⁻) produced by borate
204 hydrolysis could either form non-covalent hydrogen bonds or undergo esterification to
205 form borate esters with hydroxyl groups of lignin[12].

206 As shown in **Fig. 2d**, for 5%BN, no swelling and softening occur, while the slow
207 linear deformation of the matrix is related to the thermal dilatation of the solid matrix.
208 The initial values of G' and G'' are reduced further compared to that of 3%BN. Both
209 values remain stable with lower differences upon lignin thermal conversion.



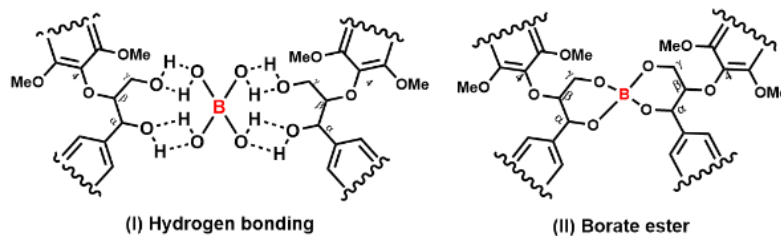
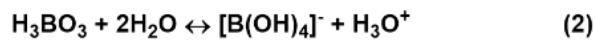
210

211

Fig. 2. The modulus and deformation curves of lignin samples measured via

212

rheometer.



213

Scheme 1. Proposed interaction mechanism between borate and lignin chains during

215

pretreatment.

216

The variation of $\tan(\delta)$ reflects the evolution of the viscoelasticity of materials[3].

217

As shown in **Fig. 3**, the peak on the $\tan(\delta)$ curve represents the tendency of lignin to

218

change from solid to liquid. It can be seen that with the increase of boron amount, the

219

transition peak (170 °C) shifts to a higher temperature with the decreased intensity

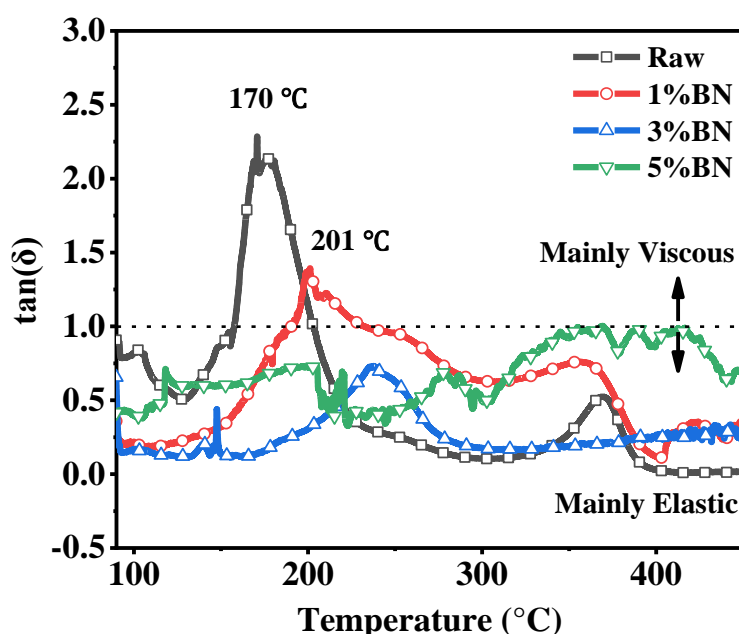
220

until it disappears completely (5%BN). This demonstrates the contribution of borates

221

to the phase stability of lignin. The line of $\tan(\delta) = 1$ divided the curve into a

222 swelling-softening stage ($\tan(\delta) > 1$) and solidification stage ($\tan(\delta) < 1$). Both raw
 223 and 1%BN showed small peaks (350~400 °C), which might be related to secondary
 224 cleavages of bonds (**Fig. 1**). Then the solidification of the matrix is accelerated with
 225 the release of volatiles, resulting in the formation of rigid char. Moreover, the peak
 226 intensity of the $\tan(\delta)$ curve of 3%BN at 150 °C is lower than that at 200 °C. The
 227 addition of boron provides a possible way to prepare high tensile strength lignin-based
 228 carbon fibers[18].



229

230 **Fig. 3.** Evolution of $\tan(\delta)$ as a function of temperature.

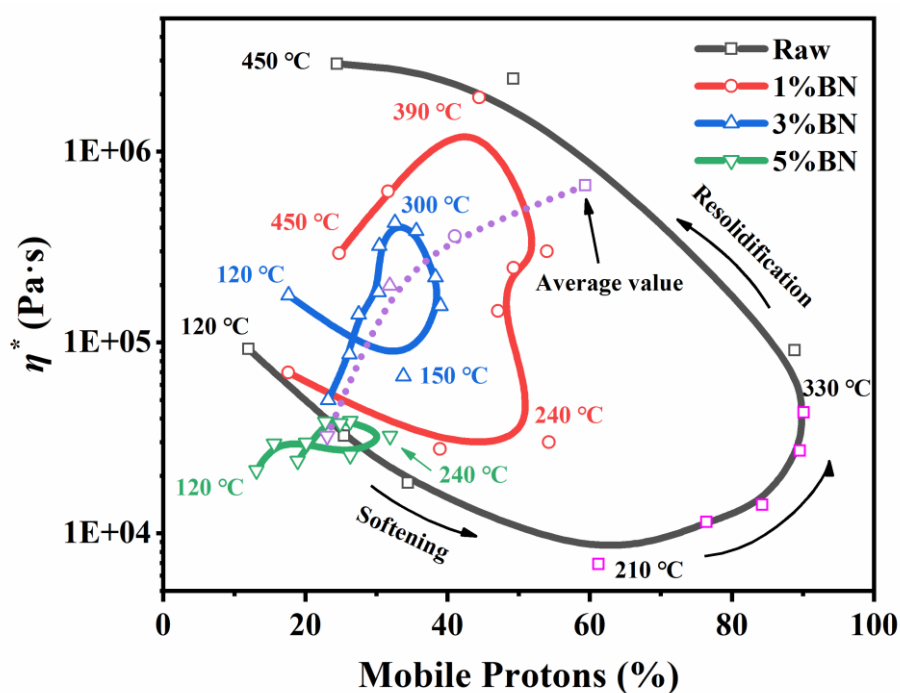
230

231 **3.3. Relation between mobile protons and complex viscosity during lignin**
 232 **pyrolysis**

233 The relation between complex viscosity ($|\eta^*|$) and mobile protons is illustrated in
 234 **Fig. 4.** For raw lignin, both mobile protons (10%~90%) and $|\eta^*|$ value ($7 \times 10^3 \sim 3 \times 10^6$)
 235 vary over a wide range. At first, the value of $|\eta^*|$ decreases with the increase of mobile
 236 protons, corresponding to the softening stage. As the temperature rises to 210 °C, the
 237 increase of the $|\eta^*|$ value indicates that the resolidification has started, although the

238 fluidity of protons still increases continuously. The decay of mobile protons might be
 239 caused by the high boiling-point liquid intermediates being entrapped in the solid
 240 “cavities”[19]. With the rearrangement, condensation, and crosslinking of the
 241 intermediates, the viscosity of the matrix increases rapidly to form a rigid char with
 242 still some mobile species present inside.

243 With boron addition, the evolution of mobile protons and complex viscosity is in a
 244 narrower range and both tend to shift to a lower value, as shown in **Fig. 4**. In
 245 particular, for 5%BN, few variations in $|\eta^*|$ value ($2 \times 10^4 \sim 4 \times 10^4$) with a lower fraction
 246 of fluid phase (10%~30%) is observed. This implies that the pre-crosslinking of
 247 borate promotes the formation of a stable rigid matrix upon lignin pyrolysis.
 248 Moreover, the decay of the mobile protons also improved with the increase of boron
 249 content, which might be related to the inhibited formation of liquid intermediates.
 250 This fundamentally explains why borate inhibits the formation of oligomers during
 251 lignin fast pyrolysis in our previous study, which is undoubtedly beneficial to improve
 252 the valorisation of bio-oil [20].



253

254 **Fig. 4.** Complex viscosity as a function of mobile protons during lignin pyrolysis.

255 **3.4. Evolution of functional groups during pyrolysis via DRIFT spectroscopy**

256 To better understand the impact of borate crosslinking on lignin functional groups
257 during pyrolysis, *in situ* DRIFT spectroscopy was applied and the evolution of typical
258 functional groups with temperature is shown in **Fig. 5**. The peak at 1125 cm^{-1} and 1210
259 cm^{-1} result from the vibration of C-O-C ether groups and the vibration of C-O in
260 phenolic hydroxyl groups, respectively. The stretching of C=O in carboxyl or carbonyl
261 groups appears at 1710 cm^{-1} , and the peaks at 1510 cm^{-1} and 1600 cm^{-1} are ascribed to
262 the vibration of C-C in aromatic rings and the vibration of C=C in conjugated alkenes,
263 respectively. In addition, a new peak was found at 1060 cm^{-1} caused by the vibration of
264 C-O-B, which demonstrates the cross-linking of hydroxyl groups between borates and
265 lignin.

266 For raw lignin, similarly, the intensity of ether bonds (**Fig. 5a**) and phenolic hydroxyl
267 groups (**Fig. 5b**) decrease with the rise of temperature and tend to be stable after $400\text{ }^{\circ}\text{C}$.
268 With the addition of 1% and 3%BN, the decreases in phenolic and ether functional
269 groups are not significantly affected. Nevertheless, as the additive content increases to
270 5%, more oxygenated groups remained in the biochar. This is in agreement with the
271 characteristic of a low condensation degree of residual char (**Fig. 2d**). Coincidentally,
272 shoulders around $150\text{ }^{\circ}\text{C}$ and $200\text{ }^{\circ}\text{C}$ are observed on the curves of functional groups of
273 raw and 1%BN lignin, respectively, corresponding to their respective softening stages
274 (**Fig. 2a** and **2b**).

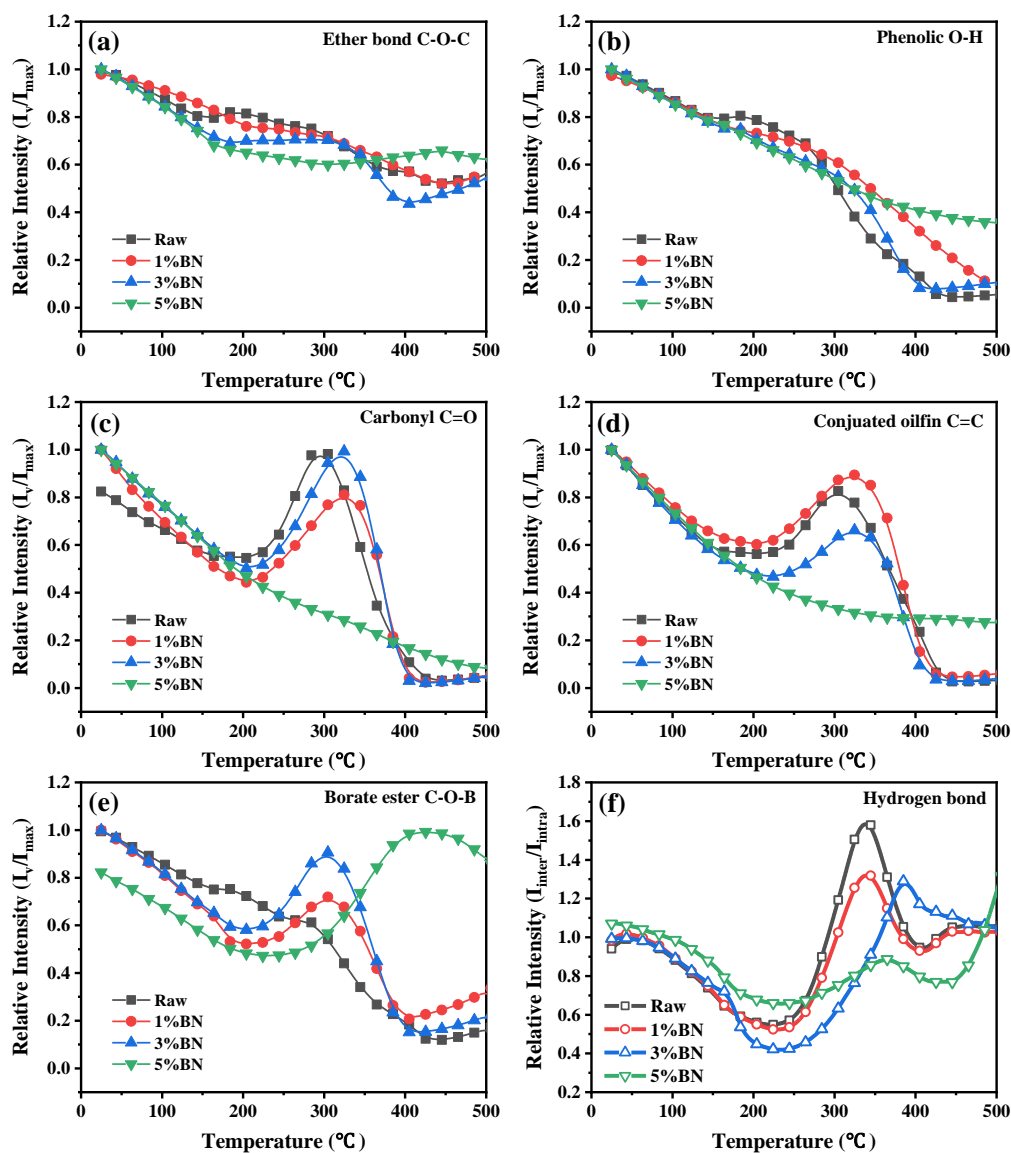
275 The variation curves of carbonyl (**Fig. 5c**) and conjugated olefin (**Fig. 5d**) are similar.
276 Their content does not decrease but increases from $200\text{ }^{\circ}\text{C}$, and decreases rapidly after
277 reaching the maximum at $300\text{ }^{\circ}\text{C}$. These groups might be formed by dehydration or
278 concerted reactions of aryl side chains[22]. With the addition of boron, the formation of

279 carbonyl and conjugated olefin are delayed or inhibited, particularly for 5%BN, which
280 is predominantly related to the shielding of reactive hydroxyl groups in lignin. This is
281 also illustrated by the decay of mobile H content (**Fig. 1**). As evidence, the decrease of
282 C-O-B before 200 °C indicates the destruction of the borate ester structures (**Fig. 5e**),
283 while the subsequent increase might be related to the formation of the new BCO
284 structures in biochar[13]. These BCO structures have a strong anchoring effect on
285 oxygen and carbon atoms, which enhance the surface polarity, and are considered to be
286 the main active sites of biochar for catalysis and adsorption[23].

287 As mentioned earlier, except to form covalent borate ester, there is also hydrogen
288 bonding between borate and lignin, which has a great effect on the thermal mobility
289 of lignin[7]. The intensity ratio between intermolecular (3200 cm^{-1}) and
290 intramolecular (3520 cm^{-1}) hydrogen bonds is shown in **Fig. 5f**. For raw lignin, the
291 relative intensity of hydrogen bonds decreases with the increase of temperature
292 (below 220 °C), suggesting that the cleavage of intermolecular hydrogen bonds is
293 faster during the lignin swelling and softening process. Subsequently, the relative
294 intensity of hydrogen bonds increased rapidly until 330 °C, indicating that the
295 breaking of intramolecular hydrogen bonds is dominant. This might be caused by
296 dehydration, depolymerization, and condensation during lignin pyrolysis, which is
297 associated with the second peak of $\tan(\delta)$ in **Fig. 3**. As the temperature continues to
298 rise, the intensity of the two hydrogen bonds tends to balance, since the amount of
299 hydrogen bonds in the rigid matrix is close to zero.

300 With boron addition, the evolution of hydrogen bonds with temperature is similar to
301 that of raw lignin. However, with the increase of boron amount, the fluctuation range
302 of the relative intensity decreases, especially the peak within 300~400 °C becomes
303 weak, indicating that the conversion of intramolecular hydrogen bonds is inhibited.

304 Besides, the impact of borate at lower content on hydrogen bond before 220 °C seems
 305 weak. This suggests that covalent borate ester (C-O-B) is the dominant binding form
 306 of borate and lignin. While for 5%BN, the initial relative intensity of hydrogen bond
 307 increased obviously, confirming the formation of new intermolecular hydrogen bonds
 308 between borate and lignin hydroxyls (**Scheme 1**).



309
 310 **Fig. 5.** (a-e) Evolution of functional groups; (f) Relative intensity of intermolecular and
 311 intramolecular hydrogen bonds as a function of temperature

312 3.5. Online analysis of volatiles during lignin pyrolysis via SPI-MS

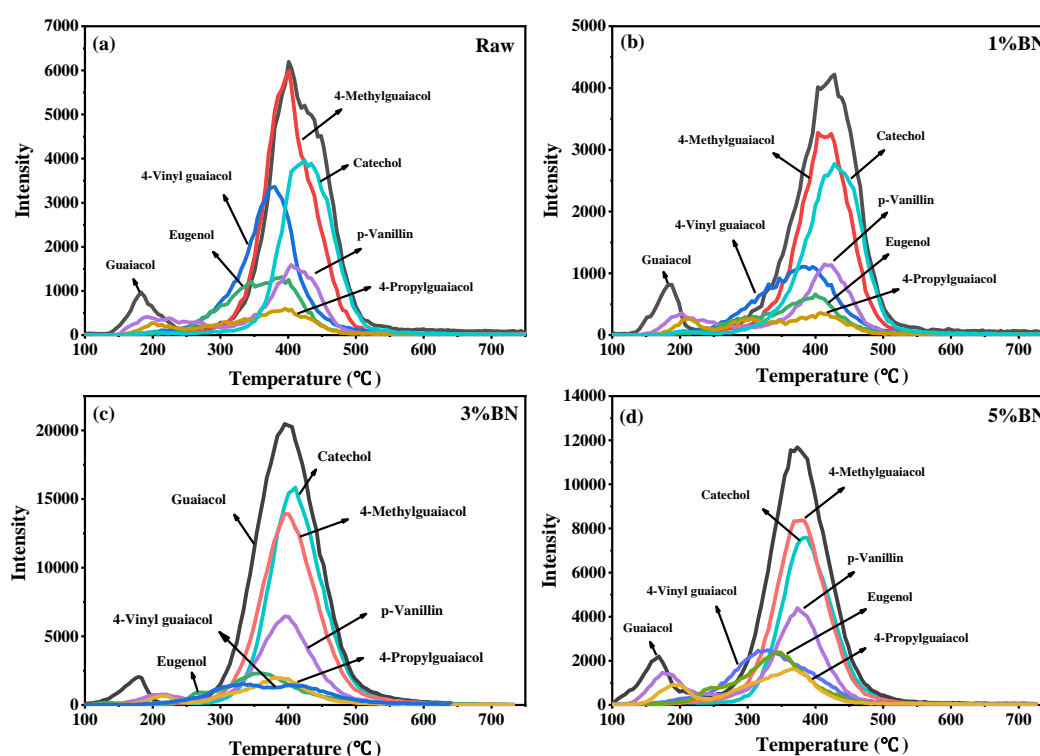
313 The release of volatiles from lignin slow pyrolysis in a microreactor was online

314 monitored using SPI-MS. The cumulative content of the main vapor products is
315 shown in **Table S4**. Guaiacol ($m/z = 124$), 4-methyl guaiacol ($m/z = 138$), catechol
316 ($m/z = 110$) and 4-vinyl guaiacol ($m/z = 150$) are the main products, and more
317 vanillin ($m/z = 152$) and eugenol ($m/z = 164$) has also been detected. With boron
318 addition, the content of phenol ($m/z = 94$), cresol ($m/z = 108$), catechol, guaiacol and
319 vanillin increases, reaching a maximum for 3%BN. This suggests that the introduction
320 of boron may be advantageous for the formation of simple phenols. However, as
321 boron content increases to 5%BN, the type and yield of volatile products are reduced,
322 which is consistent with the evolution of functional groups in the solid matrix (**Fig. 5**).

323 The evolution of typical volatiles during pyrolysis is shown in **Fig. 6**. For raw
324 lignin (**Fig. 6a**), the release profile of volatiles can be divided into two stages: 150 °C
325 ~ 250 °C and 250 °C ~ 550 °C, which correspond to the softening and solidification
326 stages of lignin, respectively (**Fig. 2a**). The smaller first release peak around 180 °C
327 (including guaiacol, vanillin, and 4-propyl guaiacol) may be formed by desorption of
328 free compounds or by the cleavage of weak bonds (like ether ones) . The larger
329 second peak near 400 °C is due to the important depolymerization reactions. In the
330 second stage, it can be seen that the release sequence of the compounds is: 4-vinyl
331 phenol and eugenol < guaiacol, 4-methyl guaiacol < vanillin and 4-propyl guaiacol <
332 catechol. When volatiles are largely released (400 °C), the mobile protons also decrease
333 (**Fig. 1**). Therefore, light volatiles may come from the secondary reactions of the
334 mobile intermediates (like oligomers present in the liquid state at 300-400°C) [1].

335 For 1%BN (**Fig. 6b**) and 3%BN (**Fig. 6c**), compare with raw lignin, there was no
336 significant change in the peak position of the products, while the signals of guaiacol
337 derivatives, such as 4-vinyl guaiacol, 4-methyl guaiacol, and eugenol, are
338 significantly attenuated. This might be because the crosslinking of borates to

339 side-chain hydroxyl groups inhibits the fracture of linkages between phenylpropane
 340 units. However, for 5% BN (**Fig. 6d**), the release peak temperatures of the volatiles
 341 decrease. This is consistent with the TGA results of our previous study [20], that
 342 higher crosslinking density leads to a forward shift of the mass loss rate peak.
 343 Furthermore, different from the raw lignin, the volatiles are rather produced from the
 344 pyrolysis of the rigid lignin-borate network due to the reduction in mobile
 345 intermediates.



346

347 **Fig. 6.** Release profile of typical volatiles during lignin pyrolysis

348

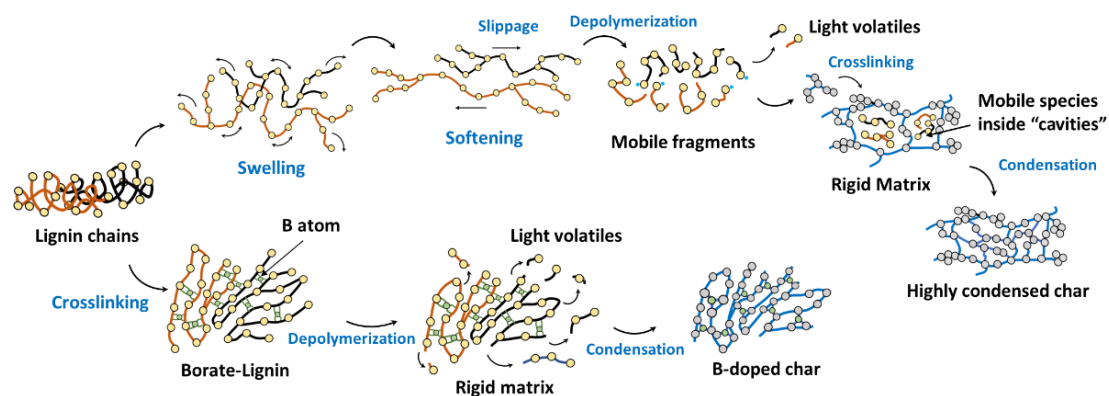
348 3.6. Physical-chemical mechanism of borate modified lignin pyrolysis

349

349 A possible pyrolysis mechanism of raw and borate modified lignin is proposed in
 350 **Scheme 2**. For raw lignin, the amorphous lignin chains become mobile at 150 °C, and
 351 then the slippage of chains starts from 170 °C due to the poor interactions of lignin
 352 molecules[25]. This corresponds to the swelling and softening of the matrix as
 353 analyzed at the macroscopic scale by in-situ rheology. Subsequently, the aryl ether

354 bonds, such as β -O-4, are cleaved as evidenced by in-situ DRIFT, resulting in the
 355 depolymerization of the lignin chain into free radical fragments with higher mobility.
 356 These intermediates are further cracked to form vapor products, or crosslinked and
 357 repolymerized to form solid char. The crosslinking of the viscous matrix entraps
 358 mobile intermediates (as analyzed by in-situ NMR) in rigid "cavities". This
 359 mechanism impedes the release of volatiles and promotes the secondary reactions of
 360 mobile species entrapped in the cavities.

361 The pretreatment with borate considerably impacts the mechanisms of lignin
 362 pyrolysis. Borate and lignin form a crosslinked network through hydrogen bonds and
 363 C-O-B bonds, which inhibit the mobility of lignin chains. The cleavage of bonds
 364 mainly occurs in a rigid matrix with less mobile transferable protons. The new BCO
 365 structure is formed in the char as evidenced by DRIFT spectra, which is consistent
 366 with our previous analysis of boron-doped char[13]. The boron-doped char presents
 367 an increased oxygen-grafting and interesting electronic properties of potential interest
 368 for high added-value applications [26].



369

370 **Scheme 2.** Proposed evolution mechanism of lignin chains during pyrolysis

371 4. Conclusions

372 This study investigates the mechanism of borate crosslinking on lignin softening
 373 and pyrolysis process by in situ physical and chemical techniques. The physical states

374 of lignin undergo glassy transition, swelling, softening, and resolidification stages.
375 For raw lignin, the mobile protons become up to 90%. The interactions formed
376 between borate and lignin include hydrogen bonding and crosslinked borate ester, the
377 latter being dominant. With the increase of boron content, the content of mobile
378 protons decreases, and the matrix stays mainly rigid with low deformation (lowered
379 swelling and shrinking). The pre-crosslinking by borate inhibits lignin softening and
380 foaming. In addition, the shielding of lignin hydroxyl groups by borate inhibits the
381 decomposition of lignin but improves the selectivity of simple phenols, and more
382 oxygenic groups remain in the solid char.

383 **Acknowledgements**

384 The authors gratefully acknowledge the financial support of the National Nature
385 Science Foundation of China (51976065), China Postdoctoral Science Foundation
386 (2018M640696 and 2019T120664) and China Scholarship Council, and the technical
387 support from the Analytical and Testing Center in Huazhong University of Science &
388 Technology (<http://atc.hust.edu.cn>).

389 **Supplementary materials**

390 Supplementary material associated with this article can be found in the online
391 version.

392 **References:**

- 393 [1] E. Terrell, L.D. Dellon, A. Dufour, E. Bartolomei, L.J. Broadbelt, M. Garcia-Perez,
394 A Review on Lignin Liquefaction: Advanced Characterization of Structure and
395 Microkinetic Modeling, *Ind. Eng. Chem.*, 59 (2019) 526-555.
- 396 [2] S. Zhou, R.C. Brown, X. Bai, The use of calcium hydroxide pretreatment to
397 overcome agglomeration of technical lignin during fast pyrolysis, *Green Chem.*, 17
398 (2015) 4748-4759.

- 399 [3] B. Shrestha, Y. le Brech, T. Ghislain, S. Leclerc, V. Carré, F. Aubriet, S. Hoppe, P.
400 Marchal, S. Pontvianne, N. Brosse, A. Dufour, A Multitechnique Characterization of
401 Lignin Softening and Pyrolysis, *ACS Sustain. Chem. Eng.*, 5 (2017) 6940-6949.
- 402 [4] J.A. Tiarks, C.E. Dedic, T.R. Meyer, R.C. Brown, J.B. Michael, Visualization of
403 physicochemical phenomena during biomass pyrolysis in an optically accessible
404 reactor, *J. Anal. Appl. Pyrolysis*, 143 (2019) 104667.
- 405 [5] S. Zhou, B. Pecha, M. van Kuppevelt, A.G. McDonald, M. Garcia-Perez, Slow and
406 fast pyrolysis of Douglas-fir lignin: Importance of liquid-intermediate formation on the
407 distribution of products, *Biomass Bioenergy*, 66 (2014) 398-409.
- 408 [6] A. Dufour, M. Castro-Diaz, N. Brosse, M. Bouroukba, C. Snape, The origin of
409 molecular mobility during biomass pyrolysis as revealed by in situ ¹H NMR
410 spectroscopy, *ChemSusChem*, 5 (2012) 1258-1265.
- 411 [7] S. Kubo, J.F. Kadla, Hydrogen bonding in lignin: a Fourier transform infrared
412 model compound study, *Biomacromolecules*, 6 (2005) 2815-2821.
- 413 [8] X. Xin, K.M. Torr, F. de Miguel Mercader, S. Pang, Insights into Preventing
414 Fluidized Bed Material Agglomeration in Fast Pyrolysis of Acid-Leached Pine Wood,
415 *Energy Fuels*, 33 (2019) 4254-4263.
- 416 [9] B.D. Stef Ghysels, Jan Van den Bulcke, Hero Jan Heeres; Mehmet Pala, Léon
417 Rohrbach, and Frederik Ronsse, Improving fast pyrolysis of lignin using three additives
418 with different modes of action, *Green Chem.*, 22 (2020) 6471-6488.
- 419 [10] J. Li, X. Bai, Z. Dong, Y. Chen, H. Yang, X. Wang, H.J.F. Chen, Influence of
420 additives on lignin agglomeration and pyrolysis behavior, *Fuel*, 263 (2020) 116629.
- 421 [11] H.W. Lee, Y.-M. Kim, J. Jae, S.M. Lee, S.-C. Jung, Y.-K. Park, The use of calcined
422 seashell for the prevention of char foaming/agglomeration and the production of
423 high-quality oil during the pyrolysis of lignin, *Renewable Energy*, 144 (2019) 147-152.

- 424 [12] N.-D. Le, M. Trogen, R.J. Varley, M. Hummel, N. Byrne, Effect of boric acid on
425 the stabilisation of cellulose-lignin filaments as precursors for carbon fibres, *Cellulose*,
426 28 (2020) 729-739.
- 427 [13] Z. Dong, H. Yang, Z. Liu, P. Chen, Y. Chen, X. Wang, H.J.F. Chen, Effect of
428 boron-based additives on char agglomeration and boron doped carbon microspheres
429 structure from lignin pyrolysis, *Fuel*, 303 (2021) 121237.
- 430 [14] G. Dai, G. Wang, K. Wang, Z. Zhou, S. Wang, Mechanism study of hemicellulose
431 pyrolysis by combining in-situ DRIFT, TGA-PIMS and theoretical calculation, *Proc.*
432 *Combust. Inst.*, 38 (2021) 4241-4249.
- 433 [15] A. Dufour, M. Castro-Díaz, P. Marchal, N. Brosse, R. Olcese, M. Bouroukba, C.
434 Snape, In Situ Analysis of Biomass Pyrolysis by High Temperature Rheology in
435 Relations with ¹H NMR, *Energy Fuels*, 26 (2012) 6432-6441.
- 436 [16] L. Chen, K. Yang, J. Huang, P. Liu, J. Yang, Y. Pan, F. Qi, L. Jia, Experimental and
437 kinetic study on flash pyrolysis of biomass via on-line photoionization mass
438 spectrometry, *Applications in Energy and Combustion Science*, 9 (2022).
- 439 [17] B. Hu, W. Xie, Y. Li, Z. Zhang, J. Liu, B. Zhang, T. Wang, Q. Lu,
440 Hydroxyl-Assisted Hydrogen Transfer Interaction in Lignin Pyrolysis: An Extended
441 Concerted Interaction Mechanism, *Energy Fuels*, 35 (2021) 13170-13180.
- 442 [18] W. Qu, J. Yang, X. Sun, X. Bai, H. Jin, M. Zhang, Towards producing high-quality
443 lignin-based carbon fibers: A review of crucial factors affecting lignin properties and
444 conversion techniques, *Int J Biol Macromol*, 189 (2021) 768-784.
- 445 [19] V. Mamleev, S. Bourbigot, M. Le Bras, J. Yvon, The facts and hypotheses relating
446 to the phenomenological model of cellulose pyrolysis, *J. Anal. Appl. Pyrolysis*, 84
447 (2009) 1-17.
- 448 [20] Z. Dong, H. Yang, Z. Liu, P. Chen, Y. Chen, X. Wang, H. Chen, S. Wang, Pyrolysis

449 of boron-crosslinked lignin: influence on lignin softening and product properties,
450 *Bioresour Technol*, (2022) 127218.

451 [21] J.-P.G. P. S. Thomas, G. F. Russell and B. J. Briscoe, FTIR study of the thermal
452 degradation of poly (vinyl alcohol), *J. Therm. Anal. Calorim.*, 64 (2001) 501-508.

453 [22] G. Dai, K. Wang, G. Wang, S. Wang, Initial pyrolysis mechanism of cellulose
454 revealed by in-situ DRIFT analysis and theoretical calculation, *Combust. Flame*, 208
455 (2019) 273-280.

456 [23] Y. Wang, M. Liu, X. Zhao, D. Cao, T. Guo, B. Yang, Insights into heterogeneous
457 catalysis of peroxymonosulfate activation by boron-doped ordered mesoporous carbon,
458 *Carbon*, 135 (2018) 238-247.

459 [24] C. Liu, Y. Deng, S. Wu, H. Mou, J. Liang, M. Lei, Study on the pyrolysis
460 mechanism of three guaiacyl-type lignin monomeric model compounds, *J. Anal. Appl.*
461 *Pyrolysis*, 118 (2016) 123-129.

462 [25] L. Wei, U.P. Agarwal, L. Matuana, R.C. Sabo, N.M. Stark, Performance of high
463 lignin content cellulose nanocrystals in poly(lactic acid), *Polymer*, 135 (2018) 305-313.

464 [26] F. Sun, Z. Qu, J. Gao, H.B. Wu, F. Liu, R. Han, L. Wang, T. Pei, G. Zhao, Y. Lu, In
465 Situ Doping Boron Atoms into Porous Carbon Nanoparticles with Increased Oxygen
466 Graft Enhances both Affinity and Durability toward Electrolyte for Greatly Improved
467 Supercapacitive Performance, *Adv. Funct. Mater.*, 28 (2018) 1804190.

468